Carotenoid Radical Cation Formation in LH2 of Purple Bacteria: A Quantum Chemical Study

Michael Wormit and Andreas Dreuw*

Institute of Physical and Theoretical Chemistry, Johann-Wolfgang Goethe University Frankfurt, Max-von-Laue-Strasse 7, D-60438 Frankfurt, Germany

Received: July 19, 2006; In Final Form: September 12, 2006

In LH2 complexes of *Rhodobacter sphaeroides* the formation of a carotenoid radical cation has recently been observed upon photoexcitation of the carotenoid S_2 state. To shed more light onto the yet unknown molecular mechanism leading to carotenoid radical formation in LH2, the interactions between carotenoid and bacteriochlorophyll in LH2 are investigated by means of quantum chemical calculations for three different carotenoids—neurosporene, spheroidene, and spheroidenone—using time-dependent density functional theory. Crossings of the calculated potential energy curve of the electron transfer state with the bacteriochlorophyll Q_x state and the carotenoid S_1 and S_2 states occur along an intermolecular distance coordinate for neurosporene and spheroidene, but for spheroidenone no crossing of the electron transfer state with the carotenoid S_1 state could be found. By comparison with recent experiments where no formation of a spheroidenone radical cation has been observed, a molecular mechanism for carotenoid radical cation formation is proposed in which it is formed via a vibrationally excited carotenoid S_1 or S* state. Arguments are given why the formation of the carotenoid radical cation does not proceed via the Q_x, S_2, or higher excited electron transfer states.

Introduction

Light-harvesting complexes play a crucial role in photosynthesis of bacteria and higher plants. They absorb most of the incident light and transfer the excitation energy to the photochemical reaction center (RC), where the excitation energy is converted into chemical energy by a series of electron transfer steps.

A few years ago, the structure of the peripheral antenna complex LH2 from *Rhodopseudomas* (*Rps.*) *acidophila* was determined by X-ray crystallography.[1,2] It revealed a circular structure consisting of nine similar subunits with one carotenoid (Car) and three bacteriochlorophyll *a* (BChl *a*) molecules embedded into two polypeptide chains. Two of the BChl *a* molecules (B850) are oriented perpendicular to the ring plane forming a strongly coupled ring along the circular structure of LH2. The third BChl *a* molecule (B800) is oriented parallel to it, constituting a second weakly coupled ring (Figure 1a). The Car molecules spanning the height of the LH2 complex (one in each subunit) interact with both BChl rings. The detailed knowledge of the structure of the LH2 complex resulted in a number of theoretical and experimental studies of its energy transfer pathways.[3−15]

The light-harvesting function of LH2 complexes is fulfilled by the BChl and the Car molecules, which together cover a large part of the visible spectrum, being vital for organisms especially under poor-light conditions. The efficiency of light-harvesting by Cars relies on their ability to transfer energy to the low-lying Q_x and Q_y states of B850 BChls, which finally transfer the excitation energy to the RC. This excitation energy transfer (EET) process depends on the properties of the low-lying excited S_1 and S_2 states, which in turn are strongly influenced by the conjugation length of the π-electrons in the carotenoid backbone and the functional groups attached to it. The S_2 state of carotenoids ($1B_u^+$ in C_{2h} symmetry) is an optically allowed state which is responsible for the characteristic shape of the absorption spectra of carotenoids at 400−550 nm, whereas the S_1 state ($2A_g^-$) is optically forbidden, and thus not directly accessible by conventional optical spectroscopy. Indeed its exact energetic position is still not known for most carotenoids. In recent experimental studies also reasons for other dark states, such as S*[16,17] and $S^{\ddagger}$,[18] have been given. These states are supposed to be located between S_1 and S_2, but their origin and properties are still strongly debated. They, as well, may be involved in the Car−BChl energy transfer in LH2 complexes.

Recent experimental studies have shown that the efficiency of Car → BChl EET via the S_2 route does not change significantly with conjugation length of the carotenoid. Typical values are 40−60%.[15,19,20] The opposite is true for the S_1-mediated pathway,[6,9] since its efficiency changes largely with conjugation length *N* (*N*: number of conjugated double bonds). Besides EET, also electron transfer (ET) from Car to BChl has been discovered recently in the LH2 complex of *Rhodobacter* (*Rb.*) *sphaeroides* after excitation of the S_2 state of the Car via the detection of a spheroidene radical cation.[21] Such ET processes are also known from other systems, like LHC-II in plants, where it is proposed to be relevant for the mechanism of nonphotochemical quenching (NPQ).[22] To study the effect of conjugation length on carotenoid radical formation and S_1-mediated energy transfer, Polívka et al.[23] have applied femtosecond spectroscopy to a series of reconstituted LH2 complexes from *Rb. sphaeroides* containing either only neurosporene (Neuro), spheroidene (Spher), or spheroidenone (Spherone) (Figure 1b). They found that the efficiencies of both processes drop with increasing conjugation length of the carotenoid. The S_1-mediated EET to the BChl Q_y state possesses efficiencies of 94% for Neuro (*N*=9), 80% for Spher (*N*=10), and 76% for

* Corresponding author. Tel: +49(69)798-29441. Fax: +49(69)798-29709. E-mail: andreas.dreuw@theochem.uni-frankfurt.de.

10.1021/jp064568r CCC: $33.50
Published on Web 10/26/2006

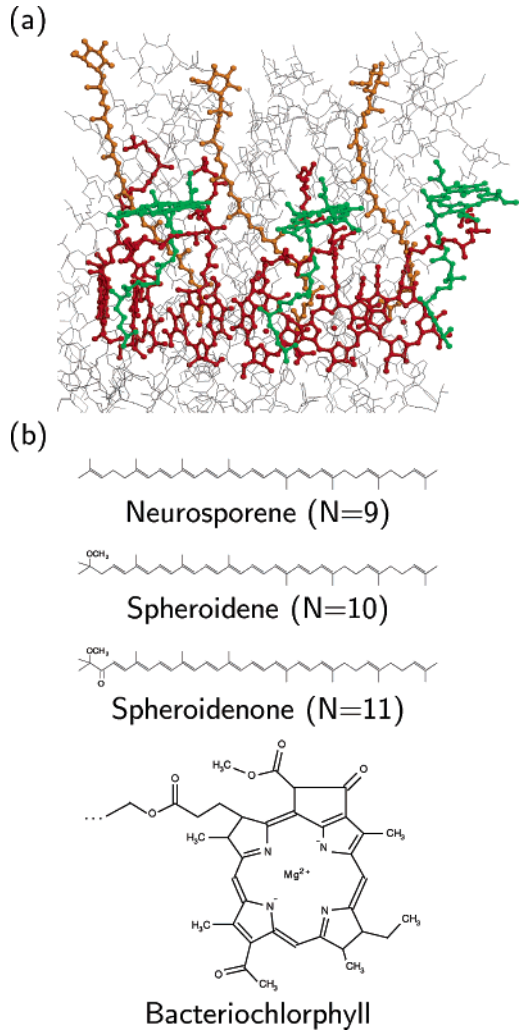

Figure 1. (a) Part of the LH2 complex of *Rps. acidophila* with the ring of B850 BChl molecules (red), the ring of B800 BChl molecules (green), and the Car molecules (orange). (b) Structures of neurosporene, spheroidene, spheroidenone, and bacteriochlorophyll used in the calculations.

Spherone (N=11). The efficiencies of carotenoid radical formation, i.e., ET from Car to BChl, have values of 10%−15% for Neuro and 5%−8% for Spher, while for Spherone no radical formation was observed. To clarify the origin of the carotenoid radical formation, the decay times of the involved excited states were analyzed. As a result, two possible precursors, a vibrationally excited S_1 state and an energetically higher ET state, were proposed. However, the detailed molecular mechanism of the ET processes in LH2 complexes remain to be established.

In this work, we investigate the Car−BChl electron transfer processes in the LH2 complex of *Rb. sphaeroides* by means of quantum chemical calculations. For this objective, we constructed molecular models for the Car−BChl systems that reproduce the observed excited states. Using these models, potential energy curves of the relevant excited states are calculated and analyzed with respect to possible ET pathways. By comparison of our results with the experimental data of Polívka et al., a mechanism for the ET process via $S_2 \rightarrow S_1 \rightarrow$ ET is suggested, which can explain the observed dependence of the ET efficiencies on the conjugation length.

Computational Methods

Our theoretical investigation comprises the construction of model complexes for the Car−BChl interactions as in the LH2 complex of *Rb. sphaeroides*, containing Neuro, Spher, and Spherone, respectively. On these model complexes calculations of the potential energy curves for the lowest electronic excited states have been performed along an intermolecular distance coordinate. For all calculations the QChem package of ab initio programs[24] has been used.

Construction of a Molecular Model. The crystal structure of the LH2 complex of *Rps. acidophila* served as a starting point for the construction of the model complexes, since no structural data of the LH2 complex of *Rb. sphaeroides* are available at present and both LH2 complexes are expected to have very similar molecular structures. From this crystal structure the protein backbone and the B850 BChl *a* molecules have been removed to build a computationally feasible model. The B850 BChls have been neglected since it was shown by Polívka et al.[21] that the electron acceptor in the Car radical cation formation, which we are mostly interested in, is the B800 BChl *a*. The influence of the protein backbone has been taken into account indirectly, as will be discussed later. From the remaining Car and B800 BChl molecules one rhodopin glucoside, the Car in LH2 of *Rps. acidophila*, and one B800 BChl have been selected to constitute the model. Although the choice of the Car is arbitrary, there are two B800 BChl molecules near a particular Car that may be involved in radical cation formation of this Car, one in the same subunit and the other (B800′) in the neighboring subunit. Both B800 BChl vary only in their position relative to the Car. Due to the strong $1/R$ distance dependence of the energy of the relevant ET states which is approximately given as $\omega_{ET} = IP - EA - 1/R$, the Car radical cation formation will occur between the Car and the spatially closest B800 BChl *a* molecule, which is the B800′. Thus we have chosen the B800′ BChl *a* molecule for our model. The end groups of rhodopin glucoside have been replaced by those of Neuro, Spher, and Spherone, respectively, and H atoms have been added, since they are not contained in the crystal structure. On these model complexes geometry optimizations have been performed to account for the inaccuracies in the crystal structures (accuracy 2.0 Å^2) and possible variations in the 3D structure of LH2 complexes of *Rps. acidophila* and *Rb. sphaeroides*. Ground state density functional theory (DFT) with the Becke−Lee−Yang−Parr (BLYP)[25] functional and 3-21G* basis set has been employed for the optimizations. We have chosen this combination of functional and basis set since it was shown that the combination yields the correct energetic ordering of the two lowest excited states of carotenoids.[26] During the optimization procedure constraints have been applied to the model complexes to incorporate spatial restrictions the neglected protein backbone would have imposed on the Car and BChl molecules. Since these spatial restrictions are indefinite, three successive optimization steps with different sets of constraints have been used. In the first step only the end groups of the Car molecules have been optimized. During the second optimization step the positions of these end groups have been kept fixed while the rest of the Car molecules has been optimized. As the last step, the whole model complexes besides the distance and orientation of the Car and BChl molecules have been optimized. After each step the optimized geometries have been evaluated by comparison of calculated electronic excited states with experimental data (Table 1, data shown only for Spher−BChl complex). As described below, the model complexes resulting from the second reoptimization have been used for the investigation.

Excited States. For the calculation of excited states the Tamm−Dancoff approximation (TDA)[27] to time-dependent density functional theory (TDDFT)[28] has been employed, since

TABLE 1: Calculated Excitation Energies (TDA/BLYP/3-21G) in eV of the Lowest Excited States of the Spher−BChl Complex at the Geometries Obtained from the Three Optimizations with Oscillator Strengths in Brackets (for comparison experimental values are given)

ex state	opt 1	opt 2	opt 3	exptl
Q_y	2.03 (0.657)	2.02 (0.688)	2.15 (1.053)	1.56
S_1	2.09 (0.011)	1.96 (0.011)	1.95 (0.003)	1.6−2.0
Q_x	2.16 (0.037)	2.17 (0.035)	2.26 (0.511)	2.10
S_2		2.28 (5.819)	2.28 (5.370)	2.42

it is at present the best applicable method for such large molecular systems, yielding reasonable excitation energies for linear polyenes.[22,26,29] As has been shown in a recent investigation,[30] the excitation energies resulting from TDA calculations on linear polyenes are very reasonable compared to highly correlated methods, although the good values are due to a fortuitous cancellation of errors. As exchange−correlation functional (xc-functional) we have chosen the BLYP functional in combination with the 3-21G basis set, which has shown to yield very good results for the calculation of electronic excited states of Car−Chl complexes.[31] The use of a larger basis set is, at present, prohibitive due to the large molecular size of the studied model complexes.

Naturally, all our calculations rely on the Born−Oppenheimer (BO) approximation, i.e., on the solution of the TDDFT equation at fixed nuclei. However, in processes that are as fast as the ones considered here with probably large nonadiabatic couplings, one may ask how well the BO states reflect reality. To study the nuclear dynamics explicitly, it would be more useful to use our adiabatic BO states and their nonadiabatic couplings as a basis to construct a diabatic basis. However, for our purposes the BO states are well suited to interpret the ongoing processes from an electronic structure point of view.

Potential energy curves of ground, valence excited, and ET states of the model complexes have been calculated along some intermolecular distance coordinate R between Car and BChl. The calculations of valence excited states have been performed using TDA/BLYP as described above, which resulted in a manifold of energetically low-lying ET states suffering from the electron transfer self-interaction problem in TDDFT.[32] A more reliable estimate of the potential energy curve of the energetically lowest ET can be obtained by utilizing the hybrid approach devised in ref 33. Employing this approach, the potential energy curve of the ET state is calculated using CIS (configuration interaction singles), since CIS yields the correct $1/R$ behavior of the potential energy curve with respect to the relevant charge separation coordinate. To incorporate the physically correct ET CIS curve into the TDDFT picture, the curve is shifted in such way that at large intermolecular distance its excitation energy matches a separately calculated ΔDFT value. The ΔDFT value is obtained as the difference of the total energies of the electronic ground state and the ET state resulting from two ground state DFT calculations employing BLYP/3-21G. The maximum overlap method has been used to force the ground state calculation to converge onto the ET state. This is a viable procedure, since for the exact xc-functional ΔDFT and TDDFT are equivalent. Thus, the high quality of TDDFT for valence excited states is combined with the correct description of ET states by CIS. The same shift is applied also for higher lying Car-to-BChl ET states.

Results

To investigate EET and ET processes in LH2 of *Rb. sphaeroides* theoretically by means of quantum chemical methods, the construction of a suitable molecular model is inevitable. As described in the previous section, the crystal structure of LH2 of *Rps. acidophila* has been used as a starting point. Following several steps of simplification, model complexes comprising Neuro−BChl, Spher−BChl, and Spherone−BChl have been constructed, which have been subjected to constraint geometry optimizations to account for uncertainties in the structures. The optimizations have been performed stepwise using constraints such that from step to step more flexibility has been added to the model complexes. By this procedure three slightly different geometries have been obtained for each model complex. Each geometry accounts for a different amount of spatial restriction due to the protein environment. To evaluate the different geometries, vertical excitation energies of the lowest excited states have been calculated using TDA/BLYP/3-21G and the results have been compared to experimental values (Table 1). The experimental values for the S_2, Q_x, and Q_y states are taken from Polívka et al.[23] The vertical excitation energy of the optically forbidden S_1 state is not accessible experimentally, and thus it can only be estimated. The excited state calculations also yielded a plethora of artificially low-lying ET states, which had to be removed. Due to these low-lying ET states and additional convergence problems, the excitation energy of the Car S_2 state at the geometry resulting from the first optimization step could not be calculated. For all optimized geometries the calculated excitation energies of the S_1, S_2, and Q_x states exhibit less than 0.2 eV deviation from the experimental values and, thus, are in acceptable agreement. Only the BChl Q_y state differs from the experimental value by 0.5 eV for the first two optimized geometries and 0.6 eV for the third optimized geometry. Since for the geometries resulting from the third optimization step the agreement of the calculated BChl states with experiment becomes worse, and additionally, the natural bent structure of the Car gets lost, these geometries are not used further. Also the geometries obtained after the first optimization step are not adequate for further investigation, because convergence problems prevent the Car S_2 state from being calculated at these geometries. Therefore, the geometries obtained after the second optimization step have been used in all subsequent calculations.

Influence of the Protein Environment. For the construction of computationally feasible model complexes it was necessary to neglect large parts of the crystal structure of the LH2 complex. Yet, in LH2 complexes the Car−BChl complex is influenced to some extent by the protein environment and the other surrounding chromophores. The spatial restrictions of the Car−BChl complex due to the environment have already been accounted for by the constraint optimizations performed on the dimer geometries. To incorporate additional effects of the surroundings, e.g., Coulombic interactions, into the model calculations, several possibilities have been tested.

One concern has been the potential influence of the protein environment on the BChl excited states which exhibit the largest deviation from the experimental excitation energies. This deviation can be attributed to one single arginine residue (βArg_{20}) close to one of the carbonyl groups of BChl (Figure 2) not contained in our model complexes. TDA/BLYP calculations of BChl together with the arginine residue result in BChl excited states with excitation energies shifted toward the experimental values.[34] However, for the model complexes comprising Car, BChl, and βArg_{20} a large number of additional ET states (Car−arginine, BChl−arginine) arise in the TDA calculations, which necessitates the calculation of a large number of excited states and thereby increases the computational cost

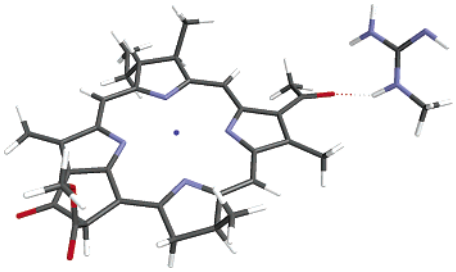

Figure 2. βArg_{20}−BChl model complex.

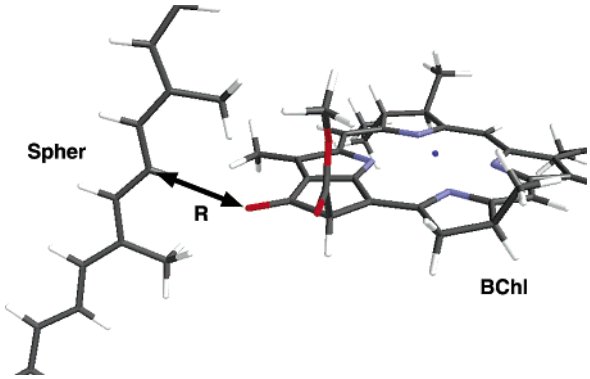

Figure 3. Intermolecular distance coordinate *R* between Car and BChl.

substantially. All these ET states suffer from the electron transfer self-interaction problem of TDDFT[32] and, thus, are found in the calculation at much too low excitation energies. Their errors can be expected to be on the order of 1−2 eV,[31] and thus, they are not relevant for the Car radical cation formation. Additionally, due to substantial mixing between these spurious ET states and real non-ET states in the TDA calculation, the interpretation of the results becomes much more complicated. Thus, the use of extended βArg_{20}−BChl−Car model complexes is not necessary. Moreover, since we are interested in the excited states of the carotenoids and the ET states, the use of the model complexes containing only Car and BChl is clearly sufficient.

Other possibilities to include the effect of the protein environment into our model calculations are the use of solvent models or the approximation of surrounding molecules by point charges. Continuum solvent models are generally problematic when utilized as a model for protein environment, since the value of the essential dielectric constant necessary to mimic the protein environment correctly is not known and probably will be different in different parts of the protein. Additionally, all codes available today implement continuum solvent models only for the ground state, but not for excited states. Similarly, the use of point charges as a model for the protein to describe the electrostatic interaction with the pigments is not feasible at the moment. Although a field of point charges can be easily constructed from the crystal structure via partial charges extracted from some molecular dynamics parameter set, calculations of the model complexes including point charges show in all cases SCF convergence failures due to overpolarization. Thus, none of the mentioned variants can be utilized to incoorporate effects of the protein environment into our model calculations.

Potential Energy Surfaces. For each of the model complexes potential energy curves have been calculated along an intermolecular distance coordinate *R*, which is defined as the distance between the ring carbonyl group of BChl and the spatially closest carbon atom of the Car (Figure 3). The distance coordinate *R* has been varied successively between 3 and 9 Å,

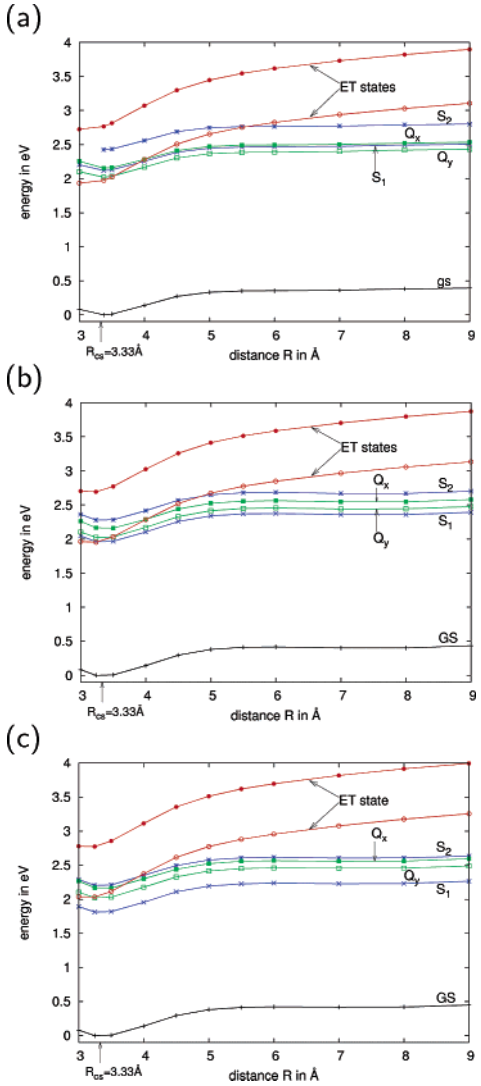

Figure 4. Potential energy curves of the ground (black line) and the lowest excited states (red: Car to BChl ET; blue: Car states; green: BChl states) of the Car−BChl complexes along the distance coordinate *R* between Car and BChl (for definition of *R* see Figure 3). (a) Neurosporene−BChl. (b) Spheroidene−BChl. (c) Spheroidenone−BChl. R_{cs} denotes the Car−BChl distance in the crystal structure.

and at each point, the valence excited and ET states have been calculated using TDA/BLYP/3-21G and the TDDFT/CIS hybrid approach, respectively, as described in the previous section. All potential energy curves of the Neuro−BChl, Spher−BChl, and Spherone−BChl complexes are displayed in Figure 4. The Car exited states (blue lines) show the experimentally observed decrease in excitation energy with increasing conjugation length *N*: the energy of the S_2 states takes values of 2.43 eV for Neuro (N=9), 2.28 eV for Spher (N=10), and 2.21 eV for Spherone (N=11) at equilibrium distance. The S_1 states behave similarly. The potential energy curves of the two lowest ET states (red lines, Figure 4) show the expected $1/R$ dependence due to the electrostatic attraction between the charged BChl and Car molecules. Analysis of the attachment and detachment densities of both ET states (Figure 5) reveals that the detachment densities are located completely on the Car, while the attachment densities have contributions only on the BChl. Consequently, both ET states correspond to excited states in which an electron has been transferred from the Car to the BChl, thus being responsible for the experimentally observed Car radical cation and a BChl radical anion.

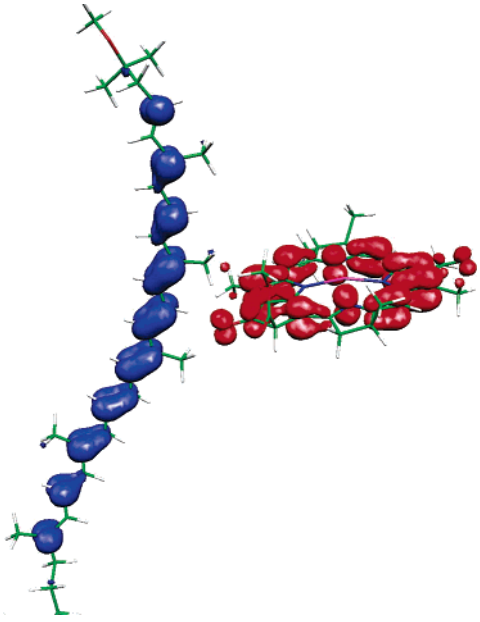

Figure 5. Detachment (blue) and attachment (red) densities of the lowest ET state of Car−BChl model complexes. Here: Spher−BChl complex. (The figure has been created using MOLEKEL[35].)

At large distances *R*, both ET states are higher in energy than any calculated valence excited state in any studied Car−BChl model complexes. The energies of the lowest ET state at these distances are about 3.2 eV for Neuro and Spher and about 3.3 eV for Spherone, corresponding to the redox potential of the Car−BChl system in the gas phase. The second ET state is higher in energy by about 0.6 eV, which reflects an excited state consisting of excited Car^+ and $BChl^-$. Due to their $1/R$ dependence, the curves of the ET states have a rather steep slope along the studied intermolecular separation coordinate compared to the curves of the valence excited states. As a result, there exist several crossings of the lowest ET state with the valence excited states for each Car, which are necessary prerequisites to make efficient ET possible. Therefore, the chosen intermolecular separation coordinate is most likely the relevant one mediating the Car → BChl ET process.[36] The second ET state, however, exhibits no crossings with any of the valence excited states. Decreasing *R*, the lowest ET state first drops below the S_2 state at 5.5 Å for Neuro, 4.8 Å for Spher, and 3.6 Å for Spherone. The shift to smaller distances with increasing conjugation length *N* is obvious. Similar behavior can be observed for the S_1 state, where the crossing with the lowest ET state is located at 3.9 Å for Neuro and at 3.3 Å for Spher, while for Spherone none of the ET states drops below the S_1 state. The lowest ET state also crosses the BChl valence excited states. At 4 Å it drops below the Q_x state in Neuro−BChl and Spher−BChl. In Spherone−BChl, however, this crossing is shifted to 3.4 Å due to the increased energy of ET states. Since in all three complexes Q_y has a constantly lower energy than Q_x by 0.13 eV, the crossings of the lowest ET state with the Q_y state are located at about 0.5 Å shorter distances, which means at 3.5 Å for Neuro and Spher and a little below 3.0 Å for Spherone. However, as stated above, the calculated energies of BChl excited states are too high compared to the experimental values. Thus, the positions of crossings of lowest ET state and BChl excited state are erroneous. Especially, the experimental value of the Q_y energy is so low that no crossing of Q_y and the lowest ET state is expected in any of the three complexes. It is also important to note that the TDA/TDDFT calculations do not yield any other low-lying excited Car states between S_1 and S_2. Thus, effects due to the experimentally observed S* state cannot be included in this study.

Discussion and Conclusions

In the femtosecond experiment by Polívka et al.[23] transient absorption spectroscopy has been used to probe the EET and ET dynamics in the LH2 complex upon excitation of the S_2 states of Neuro, Spher, and Spherone, respectively. To find a theoretical explanation for the experimental findings, it is necessary to analyze our calculated results with respect to possible energy transfer pathways from the S_2 state to the ET state.

The potential energy curves in Figure 4 show that for Neuro−BChl and Spher−BChl the curve of the lowest ET state crosses the curves of the S_1, S_2 and Q_x states and drops with decreasing intermolecular separation at some point below them. For the Spherone−BChl complex, however, this ET state crosses only the curves of the S_2 and Q_x states and has a higher energy than S_1 over the complete distance range. An ET state can in principle be populated from all the states for which a crossing with it can be found, so that at equillibrium distance these states are higher in energy than the ET state. On the basis of this energetic argument alone, in Neuro−BChl and Spher−BChl S_1, S_2 and Q_x can decay into the lowest ET state, i.e., lead to Car radical formation. On the contrary, in Spherone−BChl the population of the lowest ET state can still proceed via S_2 and Q_x, but not via the S_1 state. With the same argument the population of the second lowest ET state cannot be possible from any of the mentioned valence excited states in any of the model complexes, since it exhibits no crossings with any of these states. Thus, this state can be excluded from the subsequent discussion.

Recalling the experiment by Polívka et al.,[23] signals of the Car radical cation have been observed for the LH2 complexes with Neuro and Spher, but no signal of a Spherone radical cation has been found. Since our calculations show that the population of the ET states, i.e., radical cation formation, in the Spherone containing LH2 is in fact energetically possible via S_2 → ET and Q_x → ET, but no signal is experimentally observed, these pathways can be excluded as relevant ones. As described below, the transfer from S_2 and Q_x states to the ET state competes with other, ultrafast decay channels, which make the pathway to the ET state unfavorable. Furthermore, the S_1 → ET pathway is energetically only possible for the Neuro and Spher complexes, and indeed a radical cation is observed. Thus, it is very probable that the population of the ET state proceeds only via S_1 → ET. Although, experimentally, this electron transfer pathway has been excluded by Polívka et al.[23] due to lifetime arguments, they have pointed out that the population of the ET state is still possible via a vibrationally excited S_1 state. Equally well, the ET state might be populated via the S* state, which is not present in our calculations, but experimental arguments are given that it may be located in the relevant energy regime between S_1 and S_2. With the same reasoning as in the case of the S_1 state, the experiments suggest that the population of the ET state would have to occur via a vibrationally excited S* state.

To better understand the situation, a general look at the possible EETs and ETs in the LH2 complex is helpful. Schematic energy level diagrams for the LH2 complex can be deduced from our calculations on the different Car−BChl complexes (Figure 6). Upon photoexcitation, the S_2 state can in principle decay into five different states, which are either, via EET, the BChl excited states, Q_x and Q_y, or, via internal conversion, the Car S_1 and S* states, or, via electron transfer, the ET state. Experimentally, EET into the BChl excited states

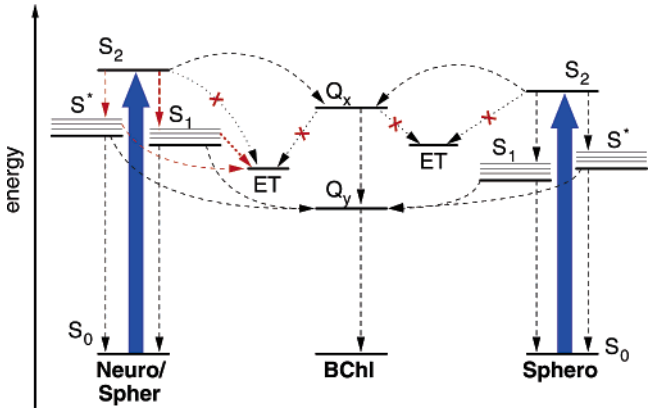

Figure 6. Schematic energy level diagram for the EET and ET processes in the Car−BChl complexes.

has a high efficiency, and 40%−60% of the S_2 excitation energy is usually transferred to the BChls within 200 fs. The rest of the S_2 population decays either into S_1, S*, or ET. However, the internal conversion to the S_1 state has been found experimentally to be also an ultrafast process with a decay time of less than 200 fs. Since the ET process occurs within 300−400 fs and the S_2 state does not exhibit such a decay component, it is very likely that the ET state is hardly populated from the S_2 state directly. The population of the ET state from the Q_x state is also not very likely, since the BChl excited states are part of the very efficient EET mechanism away from the LH2 complex. Thus, the internal conversion to the Q_y state and the EET to other BChl molecules are expected to be much faster than the decay into the ET state.[23] The only remaining excited states that can significantly populate the ET state are the S_1 and S* states of the Cars. However, both of these states exhibit two non-negligible decay channels with experimental time constants in the several picosecond range. One is the decay into the Car ground state S_0, and the other occurs via EET to the BChl Q_y state. Thus, the ET process cannot be a direct competitor of the two processes; otherwise most of the S_1 or S* population would decay into the ET state. Yet, vibrationally excited S_1 or S* states that exhibit vibrational relaxation times of less than 400 fs can populate the ET state to a small fraction (5%−15%), while the rest of the population decays into the vibrational ground state of S_1 or S* and further on into the Car ground state and BChl Q_y state. If the relevant vibrationally excited states of Spherone are lower in energy than the ET state, no formation of a Spherone radical cation would be observed. Our calculations show that the S_1 state of Spherone is 0.2 eV below the ET state at the ground state optimized geometry. The energy gap will be larger at the relaxed geometry of the Spherone S_1 state in which the system will be prior to electron transfer. Thus, it can be expected that few vibrational levels of the S_1 state are indeed below the ET state.

All these theoretical considerations have been done on the basis of comparison using simplified models of LH2 complexes with experimental findings. Yet, the models lack most of the influence of the protein and other surrounding molecules, since all our attempts to include this influence failed. However, the used TDA/TDDFT method yields reliable excited states in acceptable agreement with experimental values. To further substantiate and prove our proposed mechanism, we suggest performing a pump−deplete−probe experiment. After pumping of the Car S_2 state and a certain delay time, the S_1 state should be depleted by a second laser pulse at the excited state absorption of the Car. Then the radical cation signature should be probed. If our mechanism is correct, the radical cation signal will be diminished when the S_1 state is depleted.

Recently, carotenoid radical cation formation has also been observed as a relevant part of the high energy state quenching component (qE) of nonphotochemical quenching (NPQ) in green plants.[37,38] Upon excitation of the chlorophyll Q_y state, the formation of a zeaxanthin radical cation has been observed during NPQ, while in the unquenched state no violaxanthin radical cation has been found, although it is in principle energetically accessible.[22,31] One possibility to explain this suprising observation is the assumption that the population of the ET state, i.e., the formation of the radical cation, proceeds via the S_1 state of zeaxanthin in analogy with our suggested mechanism for LH2. Since according to the "gear-shift" model,[39] zeaxanthin is supposed to have a lower S_1 energy than violaxanthin, the S_1 state of zeaxanthin can be populated from the initially excited chlorophyll Q_y states and lead to radical cation formation via our mechanism. On the contrary, the S_1 state of violaxanthin is supposed to be higher in energy than Q_y and energetically not accessible. Hence in the unquenched state no ET state will be populated; that is, no violaxanthin radical cation will be formed.

Brief Summary and Outlook

On the basis of our quantum chemical calculations and recent experimental findings, a kinetic model has been deduced which can explain the Car radical formation in LH2 complexes. The S_2 and Q_x states could be excluded as direct precursors of the Car radical cation, since the formation of the Car radical cation is energetically possible from both states in all considered complexes, whereas experimentally no Car radical cation formation has been observed in Spherone-containing LH2 complexes. Also the formation of the Car radical cation via the S_2 state and an excited ET state could be excluded, since the second lowest ET state cannot be populated from the energetically lower S_2 state. Only for the S_1 state do the calculated potential energy curves show the experimentally expected behavior; that is, the Car radical cation formation from S_1 is energetically not possible only for the Spherone−BChl complex. Yet, due to lifetime arguments, the S_1 state has been excluded experimentally as a precursor of the ET state. Thus, the precursor of the Car radical cation is most probably a vibrationally excited S_1 or S* state, whereby the latter is expected to be energetically close to the S_1 state, but is not included in our calculations. For further support and refinement of the proposed mechanism, more accurate calculations of all excited states and calculation of reliable transition rates should be the subject of further theoretical studies.

References and Notes

(1) McDermott, G.; Prince, S. M.; Freer, A. A.; Hawthornthwaite-Lawless, A. M.; Papiz, M. Z.; Cogdell, R. J.; Isaacs, N. W. *Nature* **1995**, *374*, 517−521.

(2) Papiz, M. Z.; Prince, S. M.; Howard, T.; Cogdell, R. J.; Isaacs, N. W. *J. Mol. Biol.* **2003**, *326*, 1523−1538.

(3) Krueger, B. P.; Yom, J.; Walla, P. J.; Fleming, G. R. *Chem. Phys. Lett.* **1999**, *310*, 57−64.

(4) Krueger, B. P.; Scholes, G. D.; Jimenez, R.; Fleming, G. R. *J. Phys. Chem. B* **1998**, *102*, 2284−2292.

(5) Krueger, B. P.; Scholes, G. D.; Fleming, G. R. *J. Phys. Chem. B* **1998**, *102*, 5378−5386.

(6) Desamero, R. Z. B.; Chynwat, V.; van der Hoef, I.; Jansen, F. J.; Lugtenburg, J.; Gosztola, D.; Wasielewski, M. R.; Cua, A.; Bocian, D. F.; Frank, H. A. *J. Phys. Chem. B* **1998**, *102*, 8151−8162.

(7) Andersson, P. O.; Cogdell, R. J.; Gillbro, T. *Chem. Phys.* **1996**, *210*, 195−217.

(8) Zhang, J.-P.; Fujii, R.; Qian, P.; Inaba, T.; Mizoguchi, T.; Koyama, Y.; Onaka, K.; Watanabe, Y.; Nagae, H. *J. Phys. Chem. B* **2000**, *104*, 3683−3691.

(9) Walla, P. J.; Linden, P. A.; Hsu, C.-P.; Scholes, G. D.; Fleming, G. R. *Proc. Natl. Acad. Sci. U.S.A.* **2000**, *97*, 10808−10813.

(10) Alden, R. G.; Johnson, E.; Nagarajan, V.; Parson, W. W.; Law, C. J.; Cogdell, R. G. *J. Phys. Chem. B* **1997**, *101*, 4667−4680.

(11) Scholes, G. D.; Harcourt, R. D.; Fleming, G. R. *J. Phys. Chem. B* **1997**, *101*, 7302−7312.

(12) Scholes, G. D.; Gould, I. R.; Cogdell, R. J.; Fleming, G. R. *J. Phys. Chem. B* **1999**, *103*, 2543−2553.

(13) Sundström, V.; Pullerits, T.; van Grondelle, R. *J. Phys. Chem. B* **1999**, *103*, 2327−2346.

(14) Damjanovic, A.; Ritz, T.; Schulten, K. *Phys. Rev. E* **1999**, *59*, 3293−3311.

(15) Ricci, M.; Bradforth, S. E.; Jimenez, R.; Fleming, G. R. *Chem. Phys. Lett.* **1996**, *259*, 381−390.

(16) Gradinaru, C. C.; Kennis, J. T. M.; Papagiannakis, E.; I. van Stokkum, H. M.; Cogdell, R. J.; Fleming, G. R.; Niederman, R. A.; van Grondelle, R. *Proc. Natl. Acad. Sci. U.S.A.* **2001**, *38*, 2364−2369.

(17) Papagiannakis, E.; Kennis, J. T. M.; van Stokkum, I. H. M.; Cogdell, R. J.; van Grondelle, R. *Proc. Natl. Acad. Sci. U.S.A.* **2002**, *99*, 6017−6022.

(18) Larsen, D. S.; Papagiannakis, E.; van Stokkum, I. H. M.; Vengris, M.; Kennis, J. T. M.; van Grondelle, R. *Chem. Phys. Lett.* **2003**, *381*, 733−742.

(19) Krueger, B. P.; Scholes, G. D.; Jiminez, R.; Fleming, G. R. *J. Phys. Chem. B* **1998**, *102*, 2284−2292.

(20) Wohlleben, W.; Buckup, T.; Herek, J. L.; Codgell, R. J.; Motzkus, M. *Biophys. J.* **2003**, *85*, 442−450.

(21) Polívka, T.; Zigmantas, D.; Herek, J. L.; He, Z.; Pascher, T.; Pullertis, T.; Cogdell, R. J.; Frank, H. A.; Sundström, V. *J. Phys. Chem. B* **2002**, *106*, 11016−11025.

(22) Dreuw, A.; Fleming, G. R.; Head-Gordon, M. *J. Phys. Chem. B* **2003**, *107*, 6500−6503.

(23) Polívka, T.; Pullertis, T.; Frank, H. A.; Cogdell, R. J.; Sundström, V. *J. Phys. Chem. B* **2004**, *108*, 15398−15407.

(24) Shao, Y.; Molnar, L. F.; Jung, Y.; Kussmann, J.; Ochsenfeld, C.; Brown, S. T.; Gilbert, A. T.; Slipchenko, L. V.; Levchenko, S. V.; O'Neill, D. P.; DiStasio, R. A., Jr.; Lochan, R. C.; Wang, T.; Beran, G. J.; Besley, N. A.; Herbert, J. M.; Lin, C. Y.; Voorhis, T. V.; Chien, S. H.; Sodt, A.; Steele, R. P.; Rassolov, V. A.; Maslen, P. E.; Korambath, P. P.; Adamson, R. D.; Austin, B.; Baker, J.; Byrd, E. F. C.; Dachsel, H.; Doerksen, R. J.; Dreuw, A.; Dunietz, B. D.; Dutoi, A. D.; T. Furlani, R.; Gwaltney, S. R.; Heyden, A.; Hirata, S.; Hsu, C.-P.; Kedziora, G.; Khalliulin, R. Z.; Klunzinger, P.; Lee, A. M.; Lee, M. S.; Liang, W.; Lotan, I.; Nair, N.; Peters, B.; Proynov, E. I.; Pieniazek, P. A.; Rhee, Y. M.; Ritchie, J.; Rosta, E.; Sherrill, C. D.; Simmonett, A. C.; Subotnik, J. E.; Woodcock, H. L., III; Zhang, W.; Bell, A. T.; Chakraborty, A. K. *Phys. Chem. Chem. Phys.* **2006**, *8*, 3172−3191.

(25) Becke, A. D. *Phys. Rev. A* **1988**, *38*, 3098−3100.

(26) Hsu, C.-P.; Hirata, S.; Head-Gordon, M. *J. Phys. Chem. A* **2001**, *105*, 451−458.

(27) Hirata, S.; Head-Gordon, M. *Chem. Phys. Lett.* **1999**, *314*, 291−299.

(28) Casida, M. E. *Recent Advances in Density Functional Methods*, Part I; World Scientific: Singapore, 1995; pp 155−192.

(29) Hsu, C.-P.; Walla, P. J.; ; Head-Gordon, M.; Fleming, G. R. *J. Phys. Chem. B* **2001**, *105*, 11016−11025.

(30) Starcke, J. H.; Wormit, M.; Schirmer, J.; Dreuw, A. *J. Chem. Phys.* **2006**, accepted for publication.

(31) Dreuw, A.; Fleming, G. R.; Head-Gordon, M. *Phys. Chem. Chem. Phys.* **2003**, *5*, 3247−3256.

(32) Dreuw, A.; Head-Gordon, M. *J. Am. Chem. Soc.* **2004**, *126*, 4007−4016.

(33) Dreuw, A.; Weisman, J. L.; Head-Gordon, M. *J. Chem. Phys.* **2003**, *119*, 2943−2946.

(34) He, Z.; Sundström, V.; Pullerits, T. *J. Phys. Chem. B* **2002**, *106*, 11606−11612.

(35) Flükiger, P.; Lüthi, H. P.; Portmann, S.; Weber, J. *MOLEKEL 4.0*; Swiss Center for Scientific Computing: Manno, Switzerland, 2000.

(36) Dreuw, A.; Worth, G. A.; Cederbaum, L. S.; Head-Gordon, M. *J. Phys. Chem. B* **2004**, *108*, 19049−19055.

(37) Dreuw, A.; Fleming, G. R.; Head-Gordon, M. *Biochem. Soc. Trans.* **2005**, *33*, 858−862.

(38) Holt, N. E.; Zigmantas, D.; Valkunas, L.; Li, X.-P.; Niyogi, K. K.; Fleming, G. R. *Science* **2005**, *307*, 433−436.

(39) Frank, H. A.; Cua, A.; Chynwat, V.; Young, A.; Gosztola, D.; Wasielewski, M. R. *Photosynth. Res.* **1994**, *41*, 389−395.